Electroluminescence in Aligned Arrays of Single-Wall Carbon Nanotubes with Asymmetric Contacts

Xu Xie,[†,#] Ahmad E. Islam,[†,#] Muhammad A. Wahab,[‡,#] Lina Ye,[†,⊥] Xinning Ho,[†,¶] Muhammad A. Alam,[‡,*] and John A. Rogers[†,§,*]

[†]Department of Materials Science and Engineering and Frederick Seitz Materials Research Laboratory, University of Illinois, Urbana, Illinois 61801, United States, [‡]School of Electrical and Computer Engineering, Purdue University, West Lafayette, Indiana 47907, United States, and [§]Departments of Chemistry, Mechanical Science and Engineering, Electrical and Computer Engineering, Beckman Institute for Advanced Science and Technology, University of Illinois, Urbana, Illinois 61801, United States. [⊥]Present address: Department of Chemistry, Anhui University, Hefei 230039, China. [¶]Present address: Singapore Institute of Manufacturing Technology, Singapore 638075. [#]These authors contributed equally.

ABSTRACT

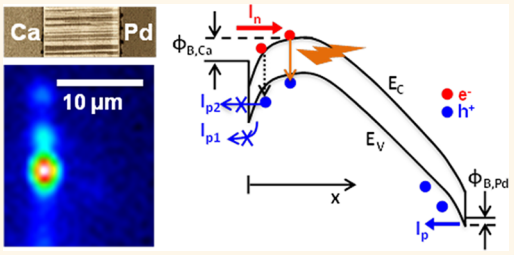

High quantum efficiencies and low current thresholds are important properties for all classes of semiconductor light emitting devices (LEDs), including nanoscale emitters based on single wall carbon nanotubes (SWNTs). Among the various configurations that can be considered in SWNT LEDs, two terminal geometries with asymmetric metal contacts offer the simplest solution. In this paper, we study, experimentally and theoretically, the mechanisms of electroluminescence in devices that adopt this design and incorporate perfectly aligned, horizontal arrays of individual SWNTs. The results suggest that exciton mediated electron–hole recombination near the lower work-function contact is the dominant source of photon emission. High current thresholds for electroluminescence in these devices result from diffusion and quenching of excitons near the metal contact.

KEYWORDS: Single-wall carbon nanotube · electroluminescence · asymmetric contact · electron–hole recombination · exciton · luminescence quenching

Past work suggests that single-wall carbon nanotubes (SWNTs) have promise as nanoscale light sources, in which emission occurs by electron–hole recombination (EHR).[1] Electroluminescence (EL) in SWNTs senses environmental changes,[1] correlates to strongly bound excitons,[2,3] and moves along the length of SWNT with applied bias,[4–7] all with emission wavelengths that depend on the SWNT diameter.[1,8] This unique combination of optoelectronic properties might make SWNT light emitters interesting for certain applications that cannot be addressed in any other way.[1,9,10] Traditionally, EL in SWNTs is achieved using field-effect transistor (FET) structures, where electrons and/or holes injected from source and drain contacts create EL in the SWNT channel (in ambipolar FETs,[4,5,11,12] and in split-gate FETs, which are also known as electrostatically doped p-i-n diodes[13]). In other forms of (unipolar) FETs,[14–17] electrons/holes created locally through impact excitation enable EL in regions with high electric field. Except for emitters fabricated as split-gate FETs,[13] which suffer from poor electron/hole injection, the power conversion efficiency in these light-emitting devices (LEDs) is generally low. Another disadvantage is that the structures all require three or more terminals. Two-terminal SWNT-based LEDs (2T-LEDs), powered by asymmetric contacts with Fermi levels near the conduction and valence bands of SWNTs offer a simpler geometry, with improved electron/hole injection.[18] Nevertheless, the threshold current for EL in such devices is relatively high compared to LEDs based on split-gate FETs.[13] The mechanisms for such high threshold currents, the spatial locations for EL along the SWNTs, and the diameter dependence of EL in 2T-LEDs remain incompletely understood.

In this paper, we analyze EL in 2T-LEDs fabricated with perfectly aligned, horizontal arrays of SWNTs grown by chemical vapor deposition (CVD) on transparent quartz substrates. A spatially resolved infrared imaging system reveals the locations of EL and the dependence of EL on diameters of the SWNTs, in a way that yields statistically relevant information. Responses from

* Address correspondence to alam@purdue.edu, jrogers@uiuc.edu.

Received for review June 9, 2012 and accepted August 6, 2012.

Published online August 06, 2012
10.1021/nn3025496

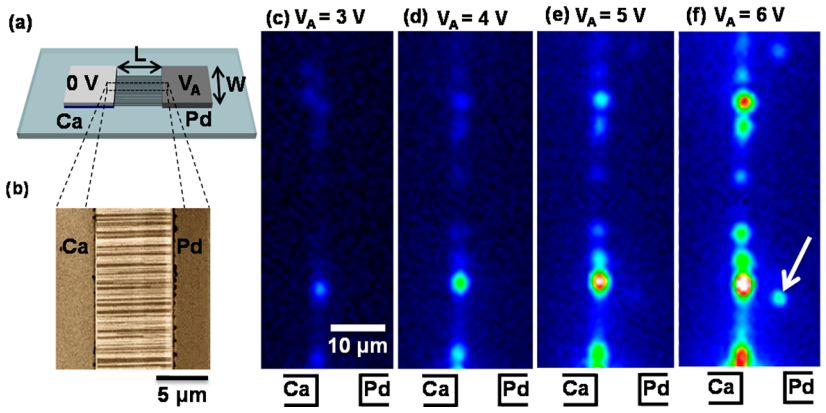

Figure 1. (a) Schematic illustration and (b) SEM image of a two-terminal light emitting device, consisting of Ca, Pd contacts, and aligned SWNTs in horizontal arrays. Devices have contact separation $L \approx 8\ \mu$m and width $W \approx 150\ \mu$m. Electroluminescence (EL) appears in such devices upon application of a bias V_A at the Pd contact, while grounding the Ca contact. (c−f) Dependence of spatial patterns of emission on V_A, measured using a InGaAs CCD camera (wavelength detection range: $\lambda \approx 800-1600$ nm). The labeled schematic illustrations at the bottom of each of these images show the positions of the contacts. Most EL appears near the Ca contact. At large V_A, it is possible to observe EL at other locations, such as near the Pd contact (*e.g.*, white arrow in panel f).

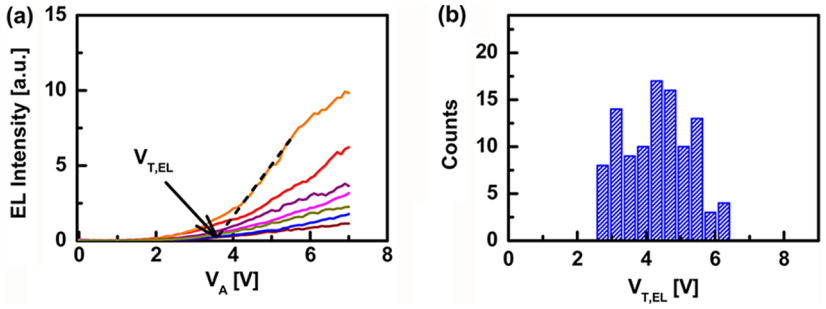

Figure 2. (a) EL intensity *vs* V_A for several, representative emission spots near the Ca contact, as obtained from Figure 1c−f. The threshold voltage for EL ($V_{T,EL}$) is defined as the *x*-axis intercept of lines (such as the dashed one shown here) drawn at the maximum of d(EL)/dV_A. (b) Distribution of $V_{T,EL}$ determined from an analysis of ∼100 emission spots.

individual SWNTs indicate that the voltages required for EL ($V_{T,EL}$) are always considerably higher than those for current injection (V_T), consistent with a high threshold current for EL.[18] We present a theoretical model that captures the details of device operation, explains the origin of EL, and postulates the quenching of excitons near the metal contact with lower work-function as the mechanism for the differences between V_T and $V_{T,EL}$. Above $V_{T,EL}$, EL occurs near the lower work-function metal contact and exhibits an emission spectrum with full-width half-maximum (FWHM) ≥ 0.06 eV.

RESULTS AND DISCUSSION

Figure 1a provides a schematic illustration of a 2T-LED that uses Ca and Pd as the contacts. A scanning electron microscope (SEM) image of part of a ∼150 μm wide device (Figure 1b) shows arrays of aligned SWNTs in between contacts separated by ∼8 μm. Separately fabricated 2T-LEDs with individual semiconducting SWNTs (s-SWNTs) allow studies of the statistical distribution of V_T. In all cases, the devices operate with the Ca contact electrically grounded and with a suitable bias (V_A) applied to the Pd contact. Figure 1 panels c−f show spatial profiles of EL at different V_A measured in air through the transparent quartz substrate with a liquid nitrogen cooled InGaAs infrared camera.[5] EL always appears near the contact with lower work-function (Ca), except for a few instances at high V_A where isolated and random EL spots occur near the higher work-function contact (Pd) (Figure 1e,f). Since the SWNT arrays have average densities of *ca.* 2−3 tubes per μm,[19] with local values that can be higher, and the diffraction limit of the IR camera is ∼1.5 μm,[5] each pixel in the EL spatial profile may include contributions from more than one SWNT. (Since metallic SWNTs only show emission at very high lateral electric fields,[20,21] all of the EL effects studied here can be assumed to originate from s-SWNTs.) Figure 2a plots the spatially integrated EL intensity as a function of V_A for different bright spots near the Ca contact of Figure 1 panels c−f. The results suggest negligible EL at $V_A < V_{T,EL}$, where the magnitude of $V_{T,EL}$ is defined by the *x*-axis intercept of a straight line drawn at maximum d(EL)/dV_A with matching slope (dotted line in Figure 2a). The values of $V_{T,EL}$ calculated from ∼100 EL spots near the Ca contact are distributed between 2.5 and 6.5 V (Figure 2b).

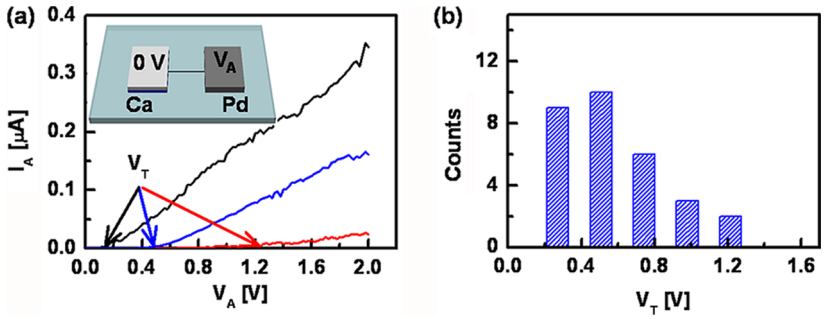

Figure 3. (a) I_A *vs* V_A characteristics for three representative devices, each of which incorporates a single s-SWNT. The arrows indicate the values of V_T for each device. (b) Distribution of V_T determined from an analysis of data collected from 30 such devices.

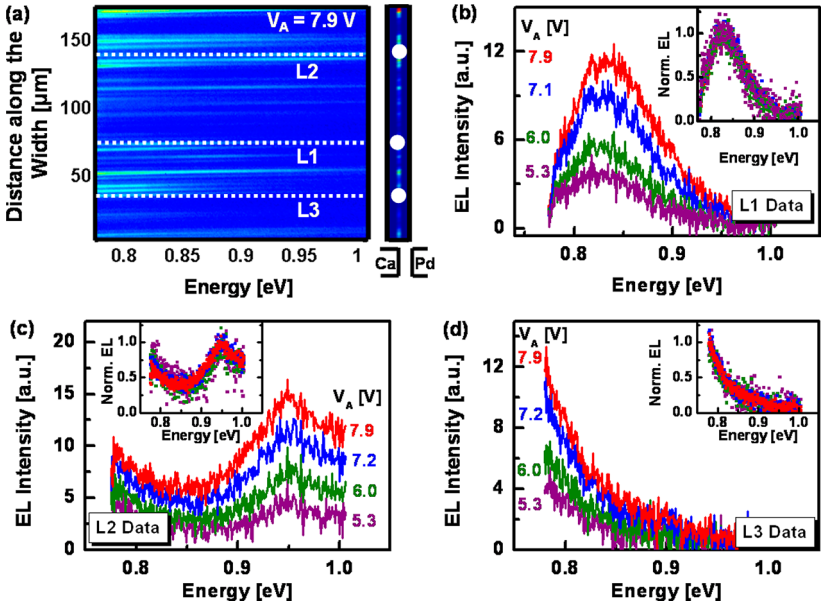

Figure 4. (a) Plot of energy-resolved EL measured along the width (*i.e.*, perpendicular to the alignment direction of the SWNT arrays) of a representative device near the Ca contact. The frame on the right shows the spatial profile of the integrated EL and the labels below the frame show the positions of the contacts. The white dots correspond to the dashed white lines on the left. EL spectra collected at various values of V_A at spots L1, L2, and L3 appear in panels b, c, and d, respectively. The insets in each case show normalized data, which suggest negligible changes in emission profiles with V_A.

The contact with low (high) work-function injects electrons (holes) into the conduction (valence) band of each s-SWNT.[18] These injected electrons and holes can recombine near the Ca contact to produce EL. (Similar EHR near metal contacts is also observed in LEDs made with ambipolar FETs and SWNT networks, where electrons injected as minority carriers from one contact recombines with holes injected as majority carriers from the other contact.[12] As explained later, a similar situation also arises in 2T-LEDs.) Therefore, the current (i.e., rate of electron/hole flow) in 2T-LEDs is correlated to EL intensity, and both are expected to have similar dependence on V_A. By contrast, current−voltage characteristics of 2T-LEDs made with individual s-SWNTs[22] show conduction at $V_A < V_{T,EL}$ (Figure 3a) and exhibit a narrow distribution in V_T (Figure 3b), where the magnitude of V_T is considered to be the *x*-axis intercept of a straight line drawn at the point of maximum dI_A/dV_A with matching slope (Supporting Information Figure 1). Differences in V_T and $V_{T,EL}$, therefore, suggest negligible conversion of EHR to EL at $V_T < V_A < V_{T,EL}$. Although dark noise in the imaging system has been identified as a reason for similar differences (*i.e.*, EL for $V_T < V_A < V_{T,EL}$ is simply undetectable) in FET-based LEDs,[23] the calculated (Supporting Information Figure 2a) and measured (Supporting Information Figure 2b) noise levels in our setups are much lower than those needed to explain the differences that we observe here.

EL spectra collected at different wavelengths (λ) provide insights into the possible roles of impact excitation[13,20,24] and blackbody radiation[25,26] in the operation. Figure 4a shows a spectrally resolved EL image collected near the Ca contact (integrated intensity over the detected wavelength range, $\lambda \approx$ 1200−1600 nm, is shown right). The EL spectra at different emission spots (Figure 4b,c) are characterized

by single or multiple Lorenzian peaks with FWHM ≥ 0.06 ± 0.0025 eV (Supporting Information Figure 3b,c). Using $E_{EL} = E_g - E_{binding}$ (where E_{EL} is the energy of EL, E_g is the bandgap of a s-SWNT, and $E_{binding}$ is the binding energy for exciton dissociation), the emission wavelengths can be correlated to the diameters of s-SWNTs. Such correlation is performed both using theoretical expressions for $E_g \approx 0.84/d$[27,28] and $E_{binding}$,[3] and using empirical expression of $E_{EL} \approx 1.11/(d + 0.11)$,[8] where the units of energy and diameter are in eV and nm, respectively. The calculation suggests s-SWNTs with smaller d (*ca.* 0.63−0.82 nm, as obtained theoretically; ca. 0.96−1.32 nm, as obtained empirically) have emission peaks (Figure 4b,c) and those with larger d (> 0.82 nm (theory), > 1.32 nm (empirical)) have emission tails (Figure 4d) within the measurement window. Although the EL intensities depend on V_A, the spectral shapes are symmetric and do not depend on V_A (insets of Figure 4b−d and Supporting Information Figures 3,4); that is, have V_A independent FWHM. Analysis shown in Supporting Information Figure 3b,c suggests that these spectra represent emission from one or multiple s-SWNTs[12] (each with FWHM *ca.* 0.06−0.09 eV) that lie within the limit of spatial resolution ($S_{res} \approx 1.5$ μm[5]) of the imaging system. The FWHMs for single s-SWNTs are somewhat larger than those reported in literature,[5,13,18] though comparable to the values observed for near contact EL,[12] possibly due to effects related to the proximity of the metal contacts to the point of emission.[11,25] The observed peak wavelengths of emission, the FWHMs, and the lack of dependence on V_A are incompatible with alternative mechanisms for emission-based on impact excitation[13,20,24] and blackbody radiation.[26] The former leads to EL typically characterized by a diameter-dependent peak wavelengths and FWHMs ≥ 0.1 eV, which remain steady and increase, respectively, with increasing V_A.[13,20,24] Blackbody effects, by contrast, involve wavelengths and FWHMs, which decrease and increase, respectively, with increasing V_A.[26] By Wein's law,[29] the temperatures of the SWNTs would need to be unrealistically high (~1500 °C) in order for radiation to appear in the experimentally observed window. In addition, emission at such temperatures would, by Planck's law,[29] have spectral widths of ~eV.[26]

To summarize the experimental findings of Figures 1−4: (i) EL occurs near the lower work-function contact, (ii) EL has a large current threshold, and (iii) EL parameters (such as V_T, $V_{T,EL}$) are characterized by statistical distributions. A theoretical framework based on a self-consistent solution of the Poisson and drift-diffusion equations (Supporting Information Figure 5) can account for these experimental observations in a way that connects EL parameters to intrinsic properties of s-SWNTs. Solution of the three-dimensional Poisson equation captures effects of the thicknesses and widths of the contacts through their influence on the electrostatics. The solution of the drift-diffusion equation describes one-dimensional carrier transport along the s-SWNTs. The mobility model[30] used in the drift-diffusion equation was calibrated against experimental measurements reported elsewhere.[30,31] To facilitate rapid simulation, carrier densities were calculated using simple analytical equations[32,33] for different positions of the Fermi levels within the bandgaps of s-SWNTs (Supporting Information Figure 6). In addition, simulation captures the influence of (oxygen and water induced) negatively charged interface defects[34,35] on the electrostatics of s-SWNT by doping the s-SWNTs with acceptors (simulation steps are detailed in the Methods section).

Figure 5a illustrates the current conduction and EL mechanisms for 2T-LEDs. Differences in the work functions of the contacts (5.1 eV for Pd[36] and 3.5 eV for Ca[37−39]) enable injection of electrons and holes from the two sides of the devices, when V_A is above V_T. (As shown in the inset of Supporting Information Figure 7b, V_T decreases with increasing s-SWNT diameter, due to a reduction in the bandgap, and by consequence, the electron barrier near the Ca contact ($\Phi_{B,Ca}$), and the hole barrier near the Pd contact ($\Phi_{B,Pd}$).) Simulation suggests that injected holes from the Pd side reach the Ca contact and cannot flow over (current component I_{p1} in Figure 5a) or tunnel through (I_{p2} in Figure 5a) the Schottky barrier near the Ca contact, whereas injected electrons from the Ca side remain near the metal contact because of the energy barrier $\Phi_{B,Ca}$. As a result, most carriers recombine near the Ca contact (Figure 5b), where exciton formation precedes photon emission. (Strong electron−hole interactions during EHR in one-dimensional s-SWNTs lead to excitons[2] with diameter dependent binding energies.[3]) However, only a fraction of these excitons contribute to EL. At low V_A, $\Phi_{B,Ca}$ is much larger than k_BT/q (Figure 5c), where k_B is the Boltzmann constant and q is electron charge, that restricts EHR near the Ca contact (Figure 5d). Excitons formed near the Ca contact can diffuse, with diffusion lengths of *ca.* 9−600 nm,[40−43] toward the Ca contact, where they are quenched, thereby suppressing EL. (Such quenching effects have been studied extensively in the context of organic optoelectronic devices.[44,45]) Quenching can also occur near the Ca contact *via* unintentional doping of the SWNT,[42,46] or due to exciton−exciton annihilation.[17] In the simulation, we consider such exciton quenching up to L_q = 250 nm away from the Ca contact. As V_A increases above $V_{T,EL}$, $\Phi_{B,Ca}$ decreases and becomes comparable to k_BT/q (Figure 5c). In this circumstance, electron flow extends further away from the quenching sites through thermal excitation, thereby leading to EHR in those regions. Excitons formed in these regions can recombine and result in EL. The s-SWNT diameter controls the magnitude of $\Phi_{B,Ca}$ at

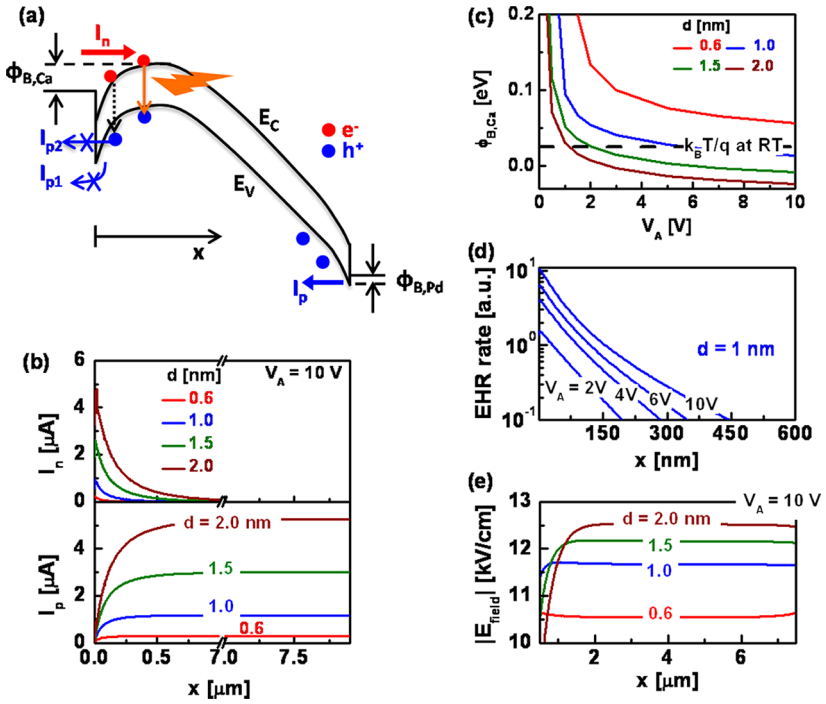

Figure 5. (a) Schematic illustration of the energy band diagram (E_C, conduction band; E_V, valence band) *vs* distance (x) along a s-SWNT in a device with Ca and Pd contacts on the left and right, respectively. (b) Computed currents associated with electrons (I_n) and holes (I_p) for s-SWNTs with different diameters (d) suggest EHR and exciton generation near the Ca contact, and negligible contributions from flow of holes over the Schottky barrier (I_{p1}) or tunneling through the barrier (I_{p2}). (c) The calculated electron barrier height near the Ca contact ($\Phi_{B,Ca}$) decreases with V_A and becomes comparable to k_BT/q at room temperature (RT) for large d. (d) Plot of calculated EHR rate *vs* x suggests that exciton generation can occur at positions beyond a quenching length ($L_q \approx 250$ nm) for $V_A > V_{T,EL}$ (≈ 2.4 V for $d = 1$ nm). These excitons can lead to EL. (e) Calculated electric fields (E_{field}) *vs* x for different d at $V_A \approx 10$ V (higher than the V_A used in measurements) are lower than the critical values needed for impact excitation.[28]

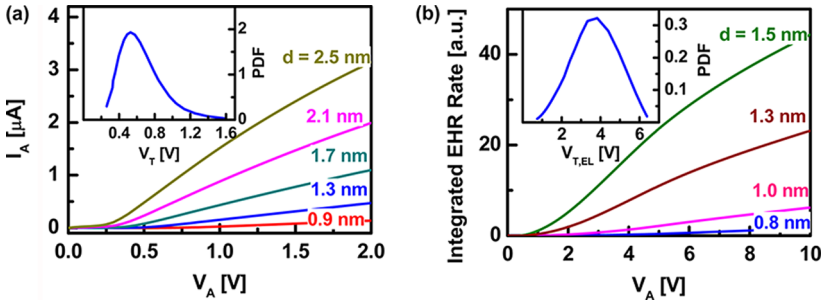

Figure 6. Simulated (a) I_A *vs* V_A and (b) integrated EHR rate *vs* V_A for s-SWNTs with different d suggest different probability distribution functions (PDF) for V_T and $V_{T,EL}$ (insets). These distributions, as well as the behaviors of I_A *vs* V_A and integrated EHR rate *vs* V_A, are similar to the experimental observation.

fixed V_A (Figure 5c), therefore, an increase in diameter results in a decrease in $V_{T,EL}$ (inset of Supporting Information Figure 7d).

Figure 6a,b shows the computed dependence of I_A on V_A and the spatially integrated (from L_q to $L_q + S_{res}$) rate for EHR in 2T-LEDs having s-SWNTs with different diameters. Simulations include the entire diameter distribution of s-SWNTs (Supporting Information Figure 7a), with plotted results selected to correspond to the range of diameters that gives rise to detectable EL, as set by the quantum efficiency (QE) of the IR camera (Supporting Information Figure 7c). The computed diameter dependence of V_T (from I_A *vs* V_A) and $V_{T,EL}$ (from integrated EHR rate *vs* V_A), the measured diameter distribution of the s-SWNTs, and the QE of the camera enable calculation of distributions in V_T and $V_{T,EL}$. The results appear in the insets of Figure 6a,b. (Supporting Information Figure 7 outlines the calculation procedures.) These simulated distributions, as well as the computed I_A-V_A and EL$-V_A$ relationships, show excellent agreement with the measurements of Figures 2 and 3. The only exception is that the results do not capture effects of saturation that are observed in I_A at large V_A for certain 2T-LEDs (Supporting Information Figure 1a).

This discrepancy is likely due to the absence of effects of contact resistance,[47] carrier backscattering,[47] or self-heating[48,49] in the models. Concerning the potential role of impact excitation, simulations suggest that the peak electric fields (E_{field}) along the s-SWNTs (even at V_A = 10 V, which is larger than the voltages used during measurement) are smaller than those[28] needed for impact excitation for s-SWNTs with d in the experimental range (0.6−3 nm) (Figure 5e). The relatively rare observations of EL near the Pd contact (arrows in Figure 1e,f) and at locations in between the Ca and Pd contacts (Supporting Information Figure 8) are likely related to defects in the SWNTs, impurities, or trapped charges[50] that can lead to sufficiently high local increases in E_{field} (hot spots).

CONCLUSIONS

We examine the mechanisms of EL in s-SWNTs using a simple two-terminal device geometry, with asymmetric contacts. Analysis of devices of this type, with both isolated SWNTs and parallel aligned arrays of them, suggests that emission results from exciton-mediated, electron−hole recombination near the lower work-function metal contact. Although the devices offer efficient injection of electrons and holes, emission is suppressed at low current levels due to quenching of excitons near the metal contact with low work function. Reducing the exciton diffusion length by enhancing the dielectric screening[3,51] may have potential to reduce the threshold current and increase the emission efficiency.

METHODS

Experiment. Fabrication of 2T-LEDs starts with the growth of aligned SWNTs *via* chemical vapor deposition (CVD) on a stable temperature (ST)-cut transparent quartz substrate using procedures described elsewhere.[52] Contacts are deposited (1 nm Ti/40 nm Pd on one side by electron beam deposition using Temescal FC-1500 and 5 nm Ca/30 nm Al on the other side in argon ambient by thermal evaporation within an MBRAUN glovebox system (H_2O < 0.1 ppm, O_2 <5 ppm)) onto the substrate in regions defined by photolithography. Here, the 1 nm layer of Ti improves adhesion of Pd with quartz[52] and the 30 nm layer of Al protects Ca against oxidation.[53] Etching of SWNTs in regions outside the device by O_2 plasma (Plasma Therm; 100 mTorr pressure, 20 sccm flow, 100 W RF power) using a photolithographically defined mask isolates the 2T-LEDs. All devices have contact separation $L \approx 8$ μm and width $W \approx 150$ μm (Figure 1a). In addition to these array-based 2T-LEDs, we built similar devices with individual s-SWNTs[22] using procedures identical to those described above. An additional step involves removal of SWNTs everywhere except for a narrow strip of width ~1.5 μm defined by photolithography. SEM imaging allows identification of devices with single SWNTs. The yield of working devices containing single s-SWNTs is ~3%.[19]

EL in 2T-LEDs is measured in air from the back of the transparent quartz substrate using a liquid nitrogen cooled InGaAs infrared camera (detected wavelength range: $\lambda \approx$ 800−1600 nm).[5] For measuring EL spectra of Figure 5, a spectrometer (with grating 150 grooves/mm and blaze 1250 nm) is placed before the IR camera to disperse the incoming light from the LED. Resultant EL spectra span a wavelength range of *ca.* 1200−1600 nm.

Modeling. Simulation of a 2T-LED containing a single s-SWNT of diameter d involves self-consistent solution of electrostatics and current flow. (Supporting Information Figure 5 outlines the procedure for simulation.) To obtain conduction (E_C) and valence (E_V) band profiles (Figure 5a), electron (n) and hole (p) concentration profiles, and E_{field} (= dE_C/dx; Figure 5e) profile along the length of the tube (x), and barriers for carrier injection ($\Phi_{B,Pd}$, $\Phi_{B,Ca}$; Figure 5a,c), we solve electrostatics using the Poisson equation:

$$\nabla\cdot(\varepsilon\nabla V) = -q(p - n - N_a^-) \quad (1)$$

where V is the electrostatic potential, ε is the dielectric constant, and N_a^- is the ionized impurity used to capture the influence of a negatively charged interface defect[34,35] on the electrostatics of s-SWNT. Supporting Information section 1 contains expressions for p, n, and N_a^-.

To simulate the electron (I_n) and hole (I_p) currents (Figure 5b), total current ($I_A = I_n + I_p$; Figure 6a), and EHR rate (Figure 5d), the following drift-diffusion equations are solved:

$$\frac{1}{q}\frac{dI_n}{dx} - R + G_{SBT,n} = 0; \quad \frac{1}{q}\frac{dI_p}{dx} + R - G_{SBT,p} = 0 \quad (2)$$

$$I_n = -qn\mu_{FE}\frac{dV}{dx} + qD_n\frac{dn}{dx}; \quad I_p = -qp\mu_{FE}\frac{dV}{dx} - qD_p\frac{dp}{dx} \quad (3)$$

In eqs 2−3, $R = \beta(np - n_i^2)$ is the EHR rate for direct band-to-band recombination,[7,54] β is the coefficient of EHR, μ_{FE} is the mobility that depends on E_{field} and d,[30,31] and $D_{n(p)}$ is the diffusion coefficient for electrons (holes). $G_{SBT,n(p)}$ in eq 2 is used to represent electron (hole) tunneling through the Schottky barriers near the contacts.[55,56] Supporting Information section 1 contains the expressions for μ_{FE}, $D_{n(p)}$, and $G_{SBT,n(p)}$. Information obtained from the self-consistent simulation of Poisson and drift-diffusion equations at different V_A are used to calculate EL intensity (Figure 6b) by integrating EHR rate from L_q to $L_q + S_{res}$ (since EHR is quenched for positions within $x = 0 \approx L_q$).

Conflict of Interest: The authors declare no competing financial interest.

Acknowledgment. We thank S. V. Rotkin (Lehigh), E. Pop (UIUC), W. P. King (UIUC), and K. L. Gross (UIUC) for valuable discussions. The work was funded by Materials Structures and Devices Focus Center (Task ID: 2051.003.4) of Semiconductor Research Corporation. EL measurements were performed in the Center for Nanoscale Materials at Argonne National Laboratory (supported by the U.S. Department of Energy, Office of Science, Office of Basic Energy Sciences, under Contract No. DE-AC02-06CH11357) with assistance from J. Zaumseil, D. J. Gosztola, and G. P. Wiederrecht. Remaining measurements were carried out in the Frederick Seitz Materials Research Laboratory Central Facilities (partially supported by the U.S. Department of Energy under Grant Nos.DE-FG02-07ER46453 and DE-FG02-07ER46671). Devices were simulated using computational support from Network of Computational Nanotechnology at Purdue University.

Supporting Information Available: Supporting Information details the measurement and simulation procedures for 2T-LED. The available materials include procedures for V_T and $V_{T,EL}$ extraction, noise correction for EL measurements, details of EL spectra, simulation details, and flowchart. This material is available free of charge *via* the Internet at http://pubs.acs.org.

REFERENCES AND NOTES

1. Avouris, P.; Freitag, M.; Perebeinos, V. Carbon-Nanotube Photonics and Optoelectronics. *Nat. Photonics* **2008**, *2*, 341–350.
2. Ando, T. Excitons in Carbon Nanotubes. *J. Phys. Soc. Jpn.* **1997**, *66*, 1066–1073.
3. Perebeinos, V.; Tersoff, J.; Avouris, P. Scaling of Excitons in Carbon Nanotubes. *Phys. Rev. Lett.* **2004**, *92*, 257402.
4. Freitag, M.; Chen, J.; Tersoff, J.; Tsang, J. C.; Fu, Q.; Liu, J.; Avouris, P. Mobile Ambipolar Domain in Carbon-Nanotube Infrared Emitters. *Phys. Rev. Lett.* **2004**, *93*, 076803.
5. Zaumseil, J.; Ho, X. N.; Guest, J. R.; Wiederrecht, G. P.; Rogers, J. A. Electroluminescence from Electrolyte-Gated Carbon Nanotube Field-Effect Transistors. *ACS Nano* **2009**, *3*, 2225–2234.
6. Abdolkader, T. M.; Alam, M. A. Diameter-Dependent Analytical Model for Light Spot Movement in Carbon Nanotube Array Transistors. *Appl. Phys. Lett.* **2011**, *98*, 063503.
7. Guo, J.; Alam, M. A. Carrier Transport and Light-Spot Movement in Carbon-Nanotube Infrared Emitters. *Appl. Phys. Lett.* **2005**, *86*, 023105.
8. Dukovic, G.; Wang, F.; Song, D. H.; Sfeir, M. Y.; Heinz, T. F.; Brus, L. E. Structural Dependence of Excitonic Optical Transitions and Band-Gap Energies in Carbon Nanotubes. *Nano Lett.* **2005**, *5*, 2314–2318.
9. Itkis, M. E.; Yu, A. P.; Haddon, R. C. Single-Walled Carbon Nanotube Thin Film Emitter-Detector Integrated Optoelectronic Device. *Nano Lett.* **2008**, *8*, 2224–2228.
10. Hogele, A.; Galland, C.; Winger, M.; Imamoglu, A. Photon Antibunching in the Photoluminescence Spectra of a Single Carbon Nanotube. *Phys. Rev. Lett.* **2008**, *100*, 217401.
11. Misewich, J. A.; Martel, R.; Avouris, P.; Tsang, J. C.; Heinze, S.; Tersoff, J. Electrically Induced Optical Emission from a Carbon Nanotube FET. *Science* **2003**, *300*, 783–786.
12. Adam, E.; Aguirre, C. M.; Marty, L.; St-Antoine, B. C.; Meunier, F.; Desjardins, P.; Menard, D.; Martel, R. Electroluminescence from Single-Wall Carbon Nanotube Network Transistors. *Nano Lett.* **2008**, *8*, 2351–2355.
13. Mueller, T.; Kinoshita, M.; Steiner, M.; Perebeinos, V.; Bol, A. A.; Farmer, D. B.; Avouris, P. Efficient Narrow-Band Light Emission from a Single Carbon Nanotube P–N Diode. *Nat. Nanotechnol.* **2010**, *5*, 27–31.
14. Perebeinos, V.; Avouris, P. Impact Excitation by Hot Carriers in Carbon Nanotubes. *Phys. Rev. B* **2006**, *74*, 121410.
15. Chen, J.; Perebeinos, V.; Freitag, M.; Tsang, J.; Fu, Q.; Liu, J.; Avouris, P. Bright Infrared Emission from Electrically Induced Excitons in Carbon Nanotubes. *Science* **2005**, *310*, 1171–1174.
16. Freitag, M.; Tsang, J. C.; Kirtley, J.; Carlsen, A.; Chen, J.; Troeman, A.; Hilgenkamp, H.; Avouris, P. Electrically Excited, Localized Infrared Emission from Single Carbon Nanotubes. *Nano Lett.* **2006**, *6*, 1425–1433.
17. Marty, L.; Adam, E.; Albert, L.; Doyon, R.; Menard, D.; Martel, R. Exciton Formation and Annihilation During 1D Impact Excitation of Carbon Nanotubes. *Phys. Rev. Lett.* **2006**, *96*, 136803.
18. Wang, S.; Zeng, Q. S.; Yang, L. J.; Zhang, Z. Y.; Wang, Z. X.; Pei, T. A.; Ding, L.; Liang, X. L.; Gao, M.; Li, Y.; *et al.* High-Performance Carbon Nanotube Light-Emitting Diodes with Asymmetric Contacts. *Nano Lett.* **2011**, *11*, 23–29.
19. Islam, A. E.; Du, F.; Ho, X.; Jin, S. H.; Dunham, S.; Rogers, J. A. Effect of Variations in Diameter and Density on the Statistics of Aligned Array Carbon-Nanotube Field Effect Transistors. *J. Appl. Phys.* **2012**, *111*, 054511.
20. Mann, D.; Kato, Y. K.; Kinkhabwala, A.; Pop, E.; Cao, J.; Wang, X. R.; Zhang, L.; Wang, Q.; Guo, J.; Dai, H. J. Electrically Driven Thermal Light Emission from Individual Single-Walled Carbon Nanotubes. *Nat. Nanotechnol.* **2007**, *2*, 33–38.
21. Xie, L. M.; Farhat, H.; Son, H. B.; Zhang, J.; Dresselhaus, M. S.; Kong, J.; Liu, Z. F. Electroluminescence from Suspended and On-Substrate Metallic Single-Walled Carbon Nanotubes. *Nano Lett.* **2009**, *9*, 1747–1751.
22. Ho, X. N.; Ye, L. N.; Rotkin, S. V.; Xie, X.; Du, F.; Dunham, S.; Zaumseil, J.; Rogers, J. A. Theoretical and Experimental Studies of Schottky Diodes That Use Aligned Arrays of Single-Walled Carbon Nanotubes. *Nano Res.* **2010**, *3*, 444–451.
23. Hibino, N.; Suzuki, S.; Wakahara, H.; Kobayashi, Y.; Sato, T.; Maki, H. Short-Wavelength Electroluminescence from Single-Walled Carbon Nanotubes with High Bias Voltage. *ACS Nano* **2011**, *5*, 1215–1222.
24. Pfeiffer, M. H. P.; Sturzl, N.; Marquardt, C. W.; Engel, M.; Dehm, S.; Hennrich, F.; Kappes, M. M.; Lemmer, U.; Krupke, R. Electroluminescence from Chirality-Sorted (9,7)-Semiconducting Carbon Nanotube Devices. *Opt. Express* **2011**, *19*, A1184–A1189.
25. Lefebvre, J.; Austing, D. G.; Finnie, P. Two Modes of Electroluminescence from Single-Walled Carbon Nanotubes. *Phys. Status Solidi RRL* **2009**, *3*, 199–201.
26. Liu, P.; Wei, Y.; Jiang, K. L.; Sun, Q.; Zhang, X. B.; Fan, S. S.; Zhang, S. F.; Ning, C. G.; Deng, J. K. Thermionic Emission and Work Function of Multiwalled Carbon Nanotube Yarns. *Phys. Rev. B* **2006**, *73*, 235412.
27. Saito, R.; Dresselhaus, G.; Dresselhaus, M. S. *Physical Properties of Carbon Nanotubes*; Imperial College Press: London, 1998.
28. Liao, A.; Zhao, Y.; Pop, E. Avalanche-Induced Current Enhancement in Semiconducting Carbon Nanotubes. *Phys. Rev. Lett.* **2008**, *101*, 256804.
29. Planck, M. On the Law of Distribution of Energy in the Normal Spectrum. *Ann. Phys.* **1901**, *4*, 553–563.
30. Perebeinos, V.; Tersoff, J.; Avouris, P. Electron–Phonon Interaction and Transport in Semiconducting Carbon Nanotubes. *Phys. Rev. Lett.* **2005**, *94*, 086802.
31. Zhou, X. J.; Park, J. Y.; Huang, S. M.; Liu, J.; McEuen, P. L. Band Structure, Phonon Scattering, and the Performance Limit of Single-Walled Carbon Nanotube Transistors. *Phys. Rev. Lett.* **2005**, *95*, 146805.
32. Marulanda, J. M.; Srivastava, A. Carrier Density and Effective Mass Calculations in Carbon Nanotubes. *Phys. Status Solidi B* **2008**, *245*, 2558–2562.
33. Akinwande, D.; Nishi, Y.; Wong, H. S. P. An Analytical Derivation of the Density of States, Effective Mass, and Carrier Density for Achiral Carbon Nanotubes. *IEEE Trans. Electron Devices* **2008**, *55*, 289–297.
34. Kim, W.; Javey, A.; Vermesh, O.; Wang, O.; Li, Y. M.; Dai, H. J. Hysteresis Caused by Water Molecules in Carbon Nanotube Field-Effect Transistors. *Nano Lett.* **2003**, *3*, 193–198.
35. Aguirre, C. M.; Levesque, P. L.; Paillet, M.; Lapointe, F.; St-Antoine, B. C.; Desjardins, P.; Martel, R. The Role of the Oxygen/Water Redox Couple in Suppressing Electron Conduction in Field-Effect Transistors. *Adv. Mater.* **2009**, *21*, 3087–3091.
36. Chen, Z. H.; Appenzeller, J.; Knoch, J.; Lin, Y. M.; Avouris, P. The Role of Metal-Nanotube Contact in the Performance of Carbon Nanotube Field-Effect Transistors. *Nano Lett.* **2005**, *5*, 1497–1502.
37. Presence of dipole near the Ca-SWNT interface[38] may increase the work-function of Ca above the commonly used value of 2.9 eV.[39]
38. He, Y.; Zhang, J. Y.; Hou, S. M.; Wang, Y.; Yu, Z. P. Schottky Barrier Formation at Metal Electrodes and Semiconducting Carbon Nanotubes. *Appl. Phys. Lett.* **2009**, *94*, 093107.
39. Michaelson, H. B. Work Function of Elements and Its Periodicity. *J. Appl. Phys.* **1977**, *48*, 4729–4733.
40. Siitonen, A. J.; Tsyboulski, D. A.; Bachilo, S. M.; Weisman, R. B. Dependence of Exciton Mobility on Structure in Single-Walled Carbon Nanotubes. *J. Phys. Chem. Lett.* **2010**, *1*, 2189–2192.
41. Moritsubo, S.; Murai, T.; Shimada, T.; Murakami, Y.; Chiashi, S.; Maruyama, S.; Kato, Y. K. Exciton Diffusion in Air-Suspended Single-Walled Carbon Nanotubes. *Phys. Rev. Lett.* **2010**, *104*, 247402.
42. Hertel, T.; Himmelein, S.; Ackermann, T.; Stich, D.; Crochet, J. Diffusion Limited Photoluminescence Quantum Yields in 1-D Semiconductors: Single-Wall Carbon Nanotubes. *ACS Nano* **2010**, *4*, 7161–7168.
43. Yoshikawa, K.; Matsuda, K.; Kanemitsu, Y. Exciton Transport in Suspended Single Carbon Nanotubes Studied by

Photoluminescence Imaging Spectroscopy. *J. Phys. Chem. C* **2010**, *114*, 4353–4356.
44. Mei, J.; Bradley, M. S.; Bulovic, V. Photoluminescence Quenching of Tris-(8-Hydroxyquinoline) Aluminum Thin Films at Interfaces with Metal Oxide Films of Different Conductivities. *Phys. Rev. B* **2009**, *79*, 235205.
45. Wu, Y.; Zhou, Y. C.; Wu, H. R.; Zhan, Y. Q.; Zhou, J.; Zhang, S. T.; Zhao, J. M.; Wang, Z. J.; Ding, X. M.; Hou, X. Y. Metal-Induced Photoluminescence Quenching of Tri-(8-Hydroxyquinoline) Aluminum. *Appl. Phys. Lett.* **2005**, *87*, 044104.
46. Dukovic, G.; White, B. E.; Zhou, Z. Y.; Wang, F.; Jockusch, S.; Steigerwald, M. L.; Heinz, T. F.; Friesner, R. A.; Turro, N. J.; Brus, L. E. Reversible Surface Oxidation and Efficient Luminescence Quenching in Semiconductor Single-Wall Carbon Nanotubes. *J. Am. Chem. Soc.* **2004**, *126*, 15269–15276.
47. Yao, Z.; Kane, C. L.; Dekker, C. High-Field Electrical Transport in Single-Wall Carbon Nanotubes. *Phys. Rev. Lett.* **2000**, *84*, 2941–2944.
48. Collins, P. G.; Hersam, M.; Arnold, M.; Martel, R.; Avouris, P. Current Saturation and Electrical Breakdown in Multi-walled Carbon Nanotubes. *Phys. Rev. Lett.* **2001**, *86*, 3128–3131.
49. Pop, E.; Mann, D. A.; Goodson, K. E.; Dai, H. J. Electrical and Thermal Transport in Metallic Single-Wall Carbon Nanotubes on Insulating Substrates. *J. Appl. Phys.* **2007**, *101*, 093710.
50. Freitag, M.; Johnson, A. T.; Kalinin, S. V.; Bonnell, D. A. Role of Single Defects in Electronic Transport Through Carbon Nanotube Field-Effect Transistors. *Phys. Rev. Lett.* **2002**, *89*, 216801.
51. Kiowski, O.; Lebedkin, S.; Hennrich, F.; Malik, S.; Rosner, H.; Arnold, K.; Surgers, C.; Kappes, M. M. Photoluminescence Microscopy of Carbon Nanotubes Grown by Chemical Vapor Deposition: Influence of External Dielectric Screening on Optical Transition Energies. *Phys. Rev. B* **2007**, *75*, 075421.
52. Xiao, J. L.; Dunham, S.; Liu, P.; Zhang, Y. W.; Kocabas, C.; Moh, L.; Huang, Y. G.; Hwang, K. C.; Lu, C.; Huang, W.; *et al.* Alignment Controlled Growth of Single-Walled Carbon Nanotubes on Quartz Substrates. *Nano Lett.* **2009**, *9*, 4311–4319.
53. Nosho, Y.; Ohno, Y.; Kishimoto, S.; Mizutani, T. N-Type Carbon Nanotube Field-Effect Transistors Fabricated by Using Ca Contact Electrodes. *Appl. Phys. Lett.* **2005**, *86*, 073105.
54. Hsieh, C. T.; Citrin, D. S.; Ruden, P. P. Recombination-Mechanism Dependence of Transport and Light Emission of Ambipolar Long-Channel Carbon-Nanotube Field-Effect Transistors. *Appl. Phys. Lett.* **2007**, *90*, 012118.
55. Ieong, M.; Solomon, P. M.; Laux, S. E.; Wong, H.-S. P.; Chidambarrao, D. Comparison of Raised and Schottky Source/Drain MOSFETs Using a Novel Tunneling Contact Model. *IEDM Technical Digest*; **1998**; pp 733−736.
56. McGuire, D. L.; Pulfrey, D. L. A Multi-scale Model for Mobile and Localized Electroluminescence in Carbon Nanotube Field-Effect Transistors. *Nanotechnology* **2006**, *17*, 5805–5811.